

Revealing the Escape Dynamics in a Hamiltonian System with Five Exits

Euaggelos E. Zotos^{1,†}, Wei Chen^{2,3,4}, Md Sanam Suraj⁵, Rajiv Aggarwal⁶ and Charanpreet Kaur⁷

Abstract The scope of this work is to reveal, by means of numerical methods, the escape process in a Hamiltonian system with five exits which describes the problem of rearrangement multichannel scattering. For determining the influence of the energy on the nature of the orbits we classify starting conditions of orbits in planes of two dimensions. All the complex basins of escape, associated with the five escape channels of the system, are illustrated by using color-coded diagrams. The distribution of time of the escape is correlated with the corresponding escape basins. The uncertainty (fractal) dimension along with the (boundary) basin entropy are computed for quantifying the degree of fractality of the dynamical system.

Keywords Hamiltonian systems, Escapes, Fractality, Basin entropy.

MSC(2010) 37N05, 37N30, 70F15.

1. Introduction

One of the most fascinating topics in nonlinear mechanics and dynamics is, without any doubt, the problem of escapes in dynamical systems (e.g., [1–17]). In these systems a finite energy of escape exists. Consequently, the test particles which are usually launched in the central region of the system find, sooner or later, one of the channels of escape in the zero velocity curve and escape. However, it should be pointed out that the existence of escape channels does not necessarily mean that all orbits must escape to infinity. This is true, taking into account that in many dynamical system bounded orbits exist for which an additional integral of motion prohibit them from escaping. Furthermore, for some orbits the required

[†]the corresponding author.

Email address: evzotos@physics.auth.gr(E. E. Zotos)

¹Department of Physics, School of Science, Aristotle University of Thessaloniki, GR-541 24, Thessaloniki, Greece

²LMB and School of Mathematical Sciences, Beihang University, Beijing 100191, China

³Peng Cheng Laboratory, Shenzhen, Guangdong 518055, China

⁴Beijing Advanced Innovation Center for Big Data and Brain Computing, Beihang University, Beijing 100191, China

⁵Department of Mathematics, Sri Aurobindo College, University of Delhi, New Delhi-110017, Delhi, India

⁶Department of Mathematics, Deshbandhu College, University of Delhi, New Delhi-110019, Delhi, India

⁷Department of Mathematics, SGTB Khalsa College, North Campus, University of Delhi, New Delhi, India

time for escape could be extremely long, in relation to the natural crossing time of the system.

It is well-known that the problem of escapes in dynamical systems is also closely related with the topic of chaotic scattering (e.g., [18]). In this case a test particle, coming outside from the system (usually from infinity), enters the scattering region, where its trajectory is altered, and then either it stays bounded to the system or escapes again to infinity. Over the years, the phenomenon of chaotic scattering has been extensively studied from the point of view of chaos theory (e.g., [19, 20, 22–24, 46]).

In dynamical systems, where escape channels are present, an important issue is to locate the escape basins, associated with the channels of escape (e.g., [3, 25–27]). The escape basins are similar to the attraction basins in dissipative systems (e.g., [28–32]) and also similar to the Newton-Raphson convergence basins (e.g., [33–35]).

For revealing the basins of escape in a dynamical system we have to scan, and therefore classify, starting conditions of orbits in planes of two dimensions. In this work, we will adopt the numerical approach successfully used in several previous papers for determining the basins of escape in simple Hamiltonian system, such as the Hénon-Heiles system (e.g., [28, 36, 37]) but also in more complicated ones, such as the restricted problem of three bodies (e.g., [38, 39]) or open billiards (e.g., [40]) and other applied leaking systems (e.g., [41]). According to this approach, the usual polar coordinates (r, ϕ) will be used for expressing the initial velocities of the orbits, in an attempt to maintain the intrinsic symmetries of the system.

Potential holes over many dimensional configuration spaces with several exit channels play an important role in reactive scattering (e.g., [42, 43]). As a typical process of reactive scattering we can think of a fragment consisting of k particles colliding with another fragment of $N - k$ particles. So we have in total a N particle system. When all particles have attractive interactions among each other, then the total potential has a minimum when all particles are close together and energy is needed to split the whole collection of particles into two or more fragments. In general, there are many possibilities to separate the system into various groups of particles and each one of these possible groupings defines one asymptotic arrangement channel. Each one of these arrangement channels has its own energy threshold where this arrangement starts to exist. For each fixed value of the energy a finite number of arrangement channels are open, i.e. energetically accessible. In our study we only think of scattering processes at moderate values of the total energy, where a description by some effective potential is appropriate. We do not consider events with the production of particle-antiparticle pairs which become relevant at very high energies. We also do not include the production of photons by the scattering process. If some of the particles are of the same type, then the energy is invariant under an exchange of these equal particles. This leads to a corresponding discrete symmetry of the dynamics in the phase space. Also the effective potential will then show this discrete symmetry. Therefore, it is relevant to study scattering potentials with discrete symmetries. For our analysis we will use a simple Hamiltonian with five escape channels, which may represent the effect of reactive scattering.

The article is structured as follows: In Section 2 we describe the mathematical formulation of the Hamiltonian system under consideration. The following Section 3 presents the main numerical outcomes of our investigation, regarding the orbital and escape dynamics of the system. In Section 4 we provide quantitative arguments about fractal degree of the Hamiltonian system, while we also compare the results of

the different methods. Our article ends with Section 5, where we give the discussion on our work.

2. Dynamical properties of the system

In the case of a perturbed harmonic oscillator, in two dimensions, the corresponding potential reads

$$V(x, y) = \frac{1}{2} (\omega_1 x^2 + \omega_2 y^2) + \epsilon V_1(x, y), \quad (2.1)$$

where the parameters ω_1 and ω_2 are the unperturbed frequencies, along the x and y axes of the oscillations respectively, while all the perturbing terms are contained in the $V_1(x, y)$ function.

For simplicity (mainly for more convenient calculations), we consider the case of the 1 : 1 resonance, that is when $\omega_1 = \omega_2 = \omega$. In addition, without the loss of the generality we may set $\omega = \epsilon = 1$.

It is well-known that the perturbation function $V_1(x, y)$ is of paramount importance, since it strongly influences the geometry of the curves of zero velocity. For our purposes, we require a dynamical system with several escape channels. An ideal scenario is the case where the zero velocity curves contain five channels of escape, thus describing the problem of rearrangement multichannel scattering (e.g., [44–46]). According to [16] the corresponding potential with five channels of escape is given by

$$V(x, y) = \frac{1}{2} (x^2 + y^2) - \left(\frac{1}{5} x^5 - 2x^3 y^2 + x y^4 \right). \quad (2.2)$$

The respective set of equations of motion of a particle with unit mass ($m = 1$) is

$$\begin{aligned} \ddot{x} &= -\frac{\partial V}{\partial x} = -V_x, \\ \ddot{y} &= -\frac{\partial V}{\partial y} = -V_y, \end{aligned} \quad (2.3)$$

where

$$\begin{aligned} V_x &= \omega^2 x - (x^4 - 6x^2 y^2 + y^4), \\ V_y &= \omega^2 y + 4xy(x^2 - y^2). \end{aligned} \quad (2.4)$$

are the derivatives of the first order of the potential.

Similarly, the derivatives of the second order are

$$\begin{aligned} V_{xx} &= \frac{\partial^2 V}{\partial x^2} = \omega^2 - 4x(x^2 - 3y^2), \\ V_{xy} &= \frac{\partial^2 V}{\partial x \partial y} = 4y(3x^2 - y^2), \\ V_{yx} &= \frac{\partial^2 V}{\partial y \partial x} = V_{xy}, \\ V_{yy} &= \frac{\partial^2 V}{\partial x^2} = \omega^2 + 4x(x^2 - 3y^2). \end{aligned} \quad (2.5)$$

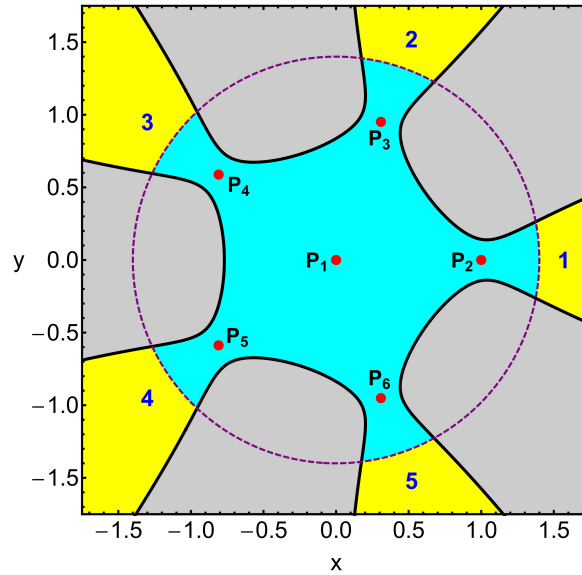


Figure 1. The open curves of zero velocity on the configuration plane (x, y) , for $E = 0.35$. P_i , $i = 1, \dots, 6$ indicate the positions of the points of equilibrium (red). The purple, dashed line delimits the scattering region (cyan), while the five escape channels are also numbered in blue. (Color figure online).

The integral of the planar motion, related to the total energy of the orbits, is given by the following Hamiltonian

$$H(x, y, \dot{x}, \dot{y}) = \frac{1}{2} (\dot{x}^2 + \dot{y}^2) + V(x, y) = E. \quad (2.6)$$

The planar motion of the test body inside the force field of the potential $V(x, y)$ defines the energetically allowed areas of motion, where $E \leq V(x, y)$.

The dynamical system, described by the potential of Eq. (2.2), has six equilibrium points P_i , $i = 1, \dots, 6$. The coordinates of the libration points are

$$\begin{aligned} P_1 : (x, y) &= (0, 0), \\ P_2 : (x, y) &= (1, 0), \\ P_3 : (x, y) &= \left(\frac{1}{2}a, \frac{1}{2}\sqrt{a+3} \right), \\ P_4 : (x, y) &= \left(\frac{1}{2}b, \frac{1}{2}\sqrt{b+3} \right), \\ P_5 : (x, y) &= \left(\frac{1}{2}b, -\frac{1}{2}\sqrt{b+3} \right), \\ P_6 : (x, y) &= \left(\frac{1}{2}a, -\frac{1}{2}\sqrt{a+3} \right), \end{aligned} \quad (2.7)$$

where $a = -(1 - \sqrt{5})/2$ and $b = -(1 + \sqrt{5})/2$.

Our numerical analysis suggests that the central equilibrium point P_1 is linearly stable, while all the other peripheral libration points P_i , $i = 2, \dots, 5$ are linearly unstable.

The value of the total energy corresponding to the equilibrium points P_i , $i = 2, \dots, 6$ is equal to $3/10$ and it is called energy of escape E_{esc} . This is true because for $E > E_{\text{esc}}$ the zero velocity curves (ZVCs), on the configuration plane (x, y) open and five channels of escape emerge. In Fig. 1 we depict the structure of the zero velocity curves for $E = 0.35$, while at the same diagram we also label the different escape channels. It is interesting to point out that geometry of the equipotential curves display a $2\pi/5$ symmetry, which is an intrinsic symmetry of the particular system.

Near the openings of the ZVCs and in the vicinity of the peripheral equilibrium points there exist highly unstable periodic orbits, which are called Lyapunov orbits.

3. Escape dynamics

For determining the character of the orbits we will adopt the numerical methods and approach used in the pioneer works of [28, 37–39]. In particular, we will classify starting conditions of orbits on the configuration (x, y) plane, for many values of the total energy E . The choice of the starting conditions is of paramount importance. As we have seen, the system with five escape channels possess a $2\pi/5$ symmetry. This symmetry should be displayed on the dynamics of the system. In addition, the five channels of escape should be equiprobable, due to the same symmetry.

The above-mentioned conditions (the symmetry as well as the equiprobable channels) are fulfilled only by the use of polar coordinates. Specifically, the condition $\dot{r} = 0$ defines a particular surface of section, of two dimensions, on the polar plane (r, ϕ) , while two disjoint parts $\dot{\phi} < 0$ and $\dot{\phi} > 0$ correspond to this surface of section. For our computations we choose the $\dot{\phi} < 0$ part, simply because our previous experience indicates that the corresponding orbital structure is more rich and therefore interesting.

For every value of E , we define a grid of 1024×1024 starting conditions (x_0, y_0) , with $R = \sqrt{x_0^2 + y_0^2} \leq 1.4$. The circular region $R \leq 1.4$ is in fact the scattering region of our system. The initial velocities of the orbits are given by the following relations

$$\begin{aligned} \dot{x}_0 &= \frac{y_0}{r} \sqrt{2(E - V(x_0, y_0))}, \\ \dot{y}_0 &= -\frac{x_0}{r} \sqrt{2(E - V(x_0, y_0))}, \end{aligned} \quad (3.1)$$

where $r = \sqrt{x_0^2 + y_0^2}$.

The starting conditions of the orbits will be categorized as: (i) orbits performing bounded orbits inside the scattering region and (ii) orbits escaping from the scattering region of the system. Furthermore, for all the escaping orbits we will keep records, regarding the particular channel of escape. An escape occurs when $r > 10$, with velocity pointing outward.

It would be very informative if we could further distinguish between order and chaos. For this task we choose the smaller alignment index (SALI) method [47]. In our computations, all the starting conditions of the orbits are integrated numerically for 10^4 time units, using a variable time step.

The orbital dynamics of the configuration plane (x, y) , for nine values of E , is revealed in Fig. 2, using color-coded diagrams. One may observe that the geometry of the several types of basins displays the $2\pi/5$ symmetry of the system. As we

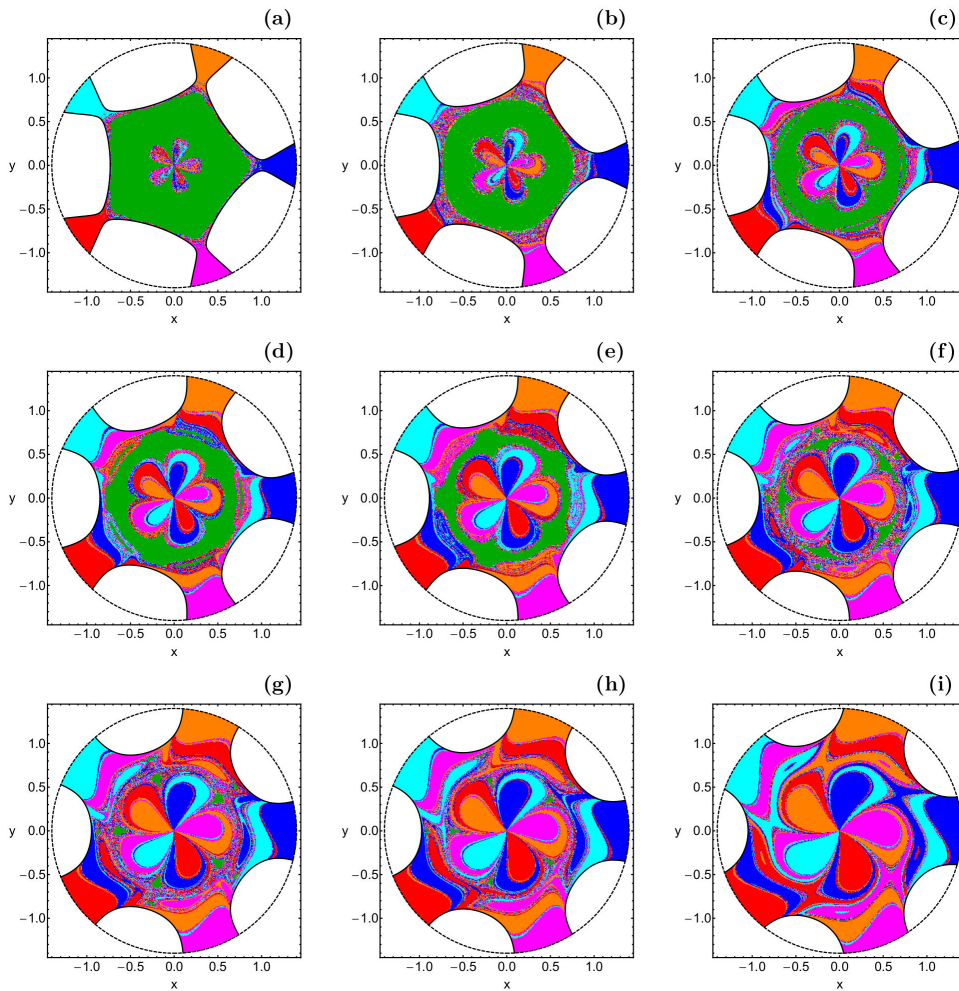


Figure 2. Color-coded diagrams depicting the dynamics of the configuration plane (x, y) , when (a): $E = 0.31$; (b): $E = 0.35$; (c): $E = 0.40$; (d): $E = 0.45$; (e): $E = 0.50$; (f): $E = 0.55$; (g): $E = 0.60$; (h): $E = 0.65$; (i): $E = 0.80$. The colors regarding the character of orbits are: chaotic trapped orbits (yellow); sticky trapped orbits (black); regular non-escaping orbits (green); escaping orbits over channel 1 (blue); escaping orbits over channel 2 (orange); escaping orbits over channel 3 (cyan); escaping orbits over channel 4 (red); escaping orbits over channel 5 (magenta). The zero velocity curves are shown in black, while the boundaries of the scattering region are indicated by black dashed line. (Color figure online).

explained earlier this is achieved by using polar coordinates, while all other types of initial conditions are not able to maintain this symmetry.

The most important changes on the orbital dynamics of the configuration plane (x, y) , with increasing value of E , are the following:

- For energies just above E_{esc} the central area of the scattering region is dominated by starting conditions which correspond to regular non-escaping orbits. However, as the value of the energy increases, the percentage of the regular orbits is reduced, while for $E > 0.80$ there is no numerical indication of bounded motion.

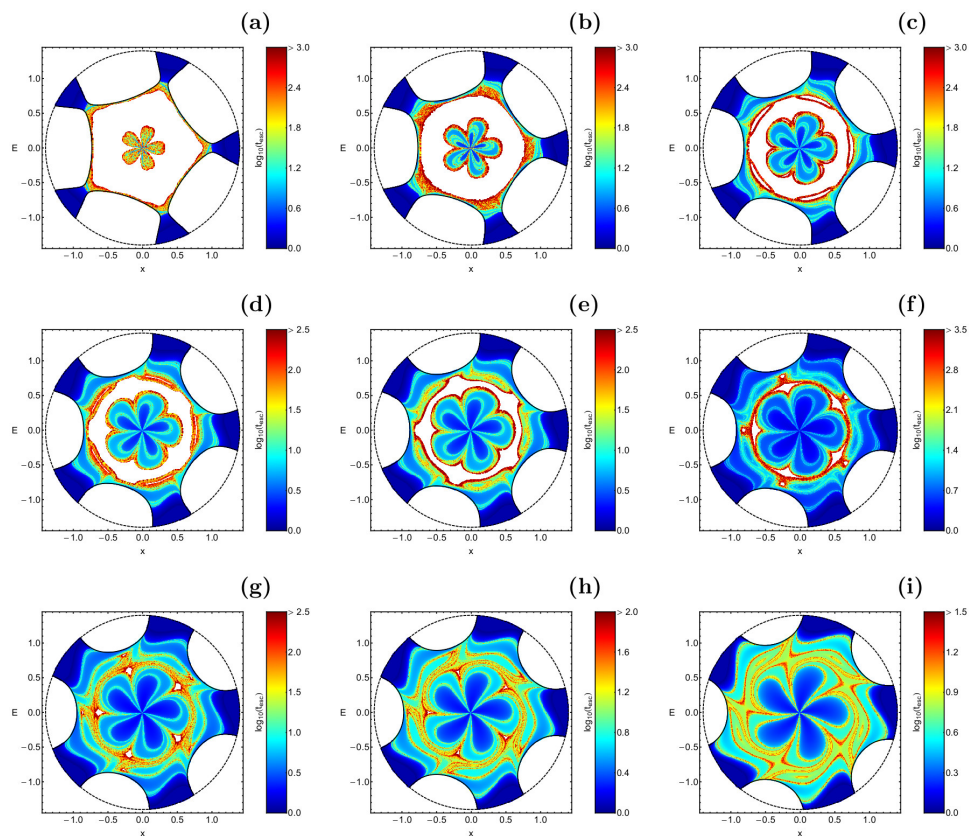


Figure 3. Distributions of the corresponding time of escape of the orbits, on the configuration plane (x, y) , for the respective values E of Fig. 2. Starting conditions of bounded (chaotic, sticky and regular) orbits are plotted in white. (Color figure online).

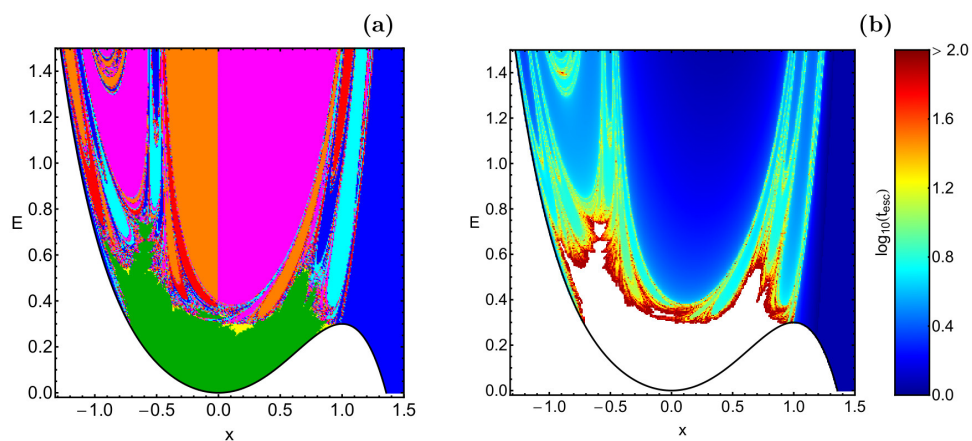


Figure 4. (a-left): Orbital dynamics of the (x, C) plane, when $E \in (0, 1.5]$ The colors are the same as in Fig. 2. (b-right): The distribution of the time of escape of the orbits. (Color figure online).

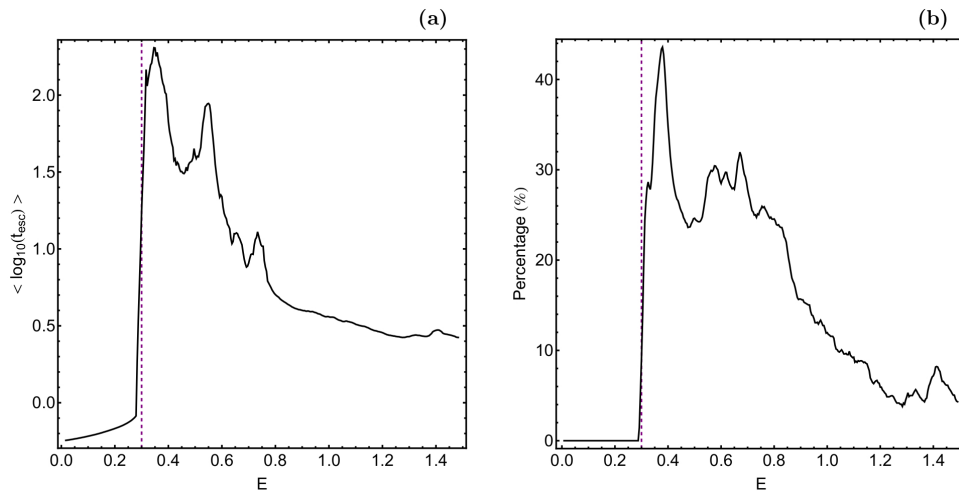


Figure 5. Parametric evolution of the (a-left): average time of escape and (b-right): percentage of areas displaying a fractal-like geometry, as a function of E . The vertical, purple, dashed line indicates the energy of escape e_{esc} . (Color figure online).

- Near the origin of the coordinates there exist a propeller-shaped structure. The size of this configuration of basins of escape is amplified, as we proceed to higher levels of E .
- The fractal areas on the configuration (x, y) space are reduced, while at the same time the basin boundaries become more smooth, with increasing width of the channels of escape.

The respective distributions of the time of escape of the orbits are illustrated in Fig. 3(a-d). It becomes evident that the highest levels of the escape time are encountered near the basin boundaries, where all the fractal structures exist.

The basin diagrams on the configuration plane (x, y) provide sufficient information on the escape dynamics of the system however, for only a specific value of E . In order to overcome this restriction we can use starting conditions on the (x, E) plane with $y = 0$.

The orbital dynamics of the (x, E) plane, when $E \in (0, 1.5]$, is illustrated in part (a) of Fig. 4, while the distribution of the time of escape of the orbits is given in part (b) of the same figure. In this type of diagram we can clearly observe the following aspects: (i) starting conditions of chaotic trapped orbits mainly appear near the boundaries of the regular basins; (ii) inside the same regions of the (x, E) plane we identify the areas with the highest degree of fractality; (iii) with increasing values of E well-formed basins of escape dominate, while at the same time all the fractal basin boundaries become smoother.

Additional useful information can also be extracted from the basin diagram on the (x, E) plane. In particular, in part (a) of Fig. 5 we present the parametric evolution of the average time of escape, as a function of E . The highest values of the time of escape are exhibited above, yet very close, to E_{esc} . For relatively high values of the energy ($E > 1$) the test particle needs no more than a couple of time units of numerical integration for escaping from the system. In part (b) of Fig. 5 we show the evolution of the percentage of the fractal area of the (x, E)

plane, compared to E . It is seen, that just above E_{esc} about 45% of the total initial conditions lie in domains which display a fractal-like geometry. The percentage of fractal regions is reduced with increasing energy and for $E > 1$ more than 90% of the areas on the (x, E) plane are covered by basins of escape, while less than 10% of the same type of plane is still occupied by fractal regions.

We would also like to present some qualitative arguments for explaining the numerical results shown in parts (a-b) of Fig. 5, which encircle the main findings of our analysis. In panel (a) we seen that in the vicinity of the energy of escape the time of escape of the orbits is very high. This however is anticipated because for these values of E the five channels of escape are very small (the corresponding width of the channel is small) and consequently the test particle should spend a considerable amount of time inside the scattering region, before it finds one of the exits and eventually escape from the system. With increasing value of E the width of the escape channels increases which leads to the observable decrease of the required escape time. A similar explanation exists also for the decrease of the fractal area. It is well known, that fractal regions mainly appear near the basin boundaries, where the unpredictability of the system is high. However, with increasing E the extent of the stability basins decreases and consequently all the fractal regions decrease.

4. The fractality of the system

In the color-coded diagrams, presented in the previous section, we have seen that near the basin boundaries there are highly fractal regions. Inside these fractal regions the fate (final state) of the orbits of the test particle is extremely sensitive. So far, when using the term “fractal” regions, we simple implied that the corresponding areas on the two-dimensional color-coded diagrams exhibit a fractal-like geometry. Nevertheless, it would be very informative to conduct additional quantitative calculations, regarding the degree of fractality of the basin diagrams, as in [36, 48].

A safe method for determining the degree of fractality is be measuring the uncertainty dimension [49], for many values of E . Fig. 6 shows the parametric evolution of the uncertainty dimension D_0 , of the configuration plane (x, y) , as a function of E . Taking into account that the corresponding color-coded basin diagrams are two-dimensional we have that $D_0 \in (1, 2)$, where $D_0 = 1$ means zero fractality, while $D_0 = 2$ implies total fractality. One may observe, that the uncertainty dimension increases rapidly, as soon as $E > E_{\text{esc}}$. The highest values of D_0 are displayed in the energy interval $(0.65, 0.8)$, while for $E > 1.1$ its value seems to saturate around 1.68 thus implying that for such high energy levels the degree of fractality is almost unaffected by the shift on the orbital energy.

In order to enrich our numerical analysis, about the fractal geometry of the basin diagrams, we decided to compute also the basin entropy, S_b , [50]. Part (a) of Fig. 7 depicts the evolution of S_b , as a function of E .

One may easily detect a striking as well as very interesting phenomenon. This phenomenon refers of course to the almost exact parametric evolution of S_b and the uncertainty dimension D_0 . Actually this is the second time that such a remarkable similarity between these two dynamical quantities is verified. The first case was in [51], where the parametric evolutions of D_0 and S_b were found to coincide. The fact that both D_0 and S_b measure, yet in a different way, the fractal degree of a

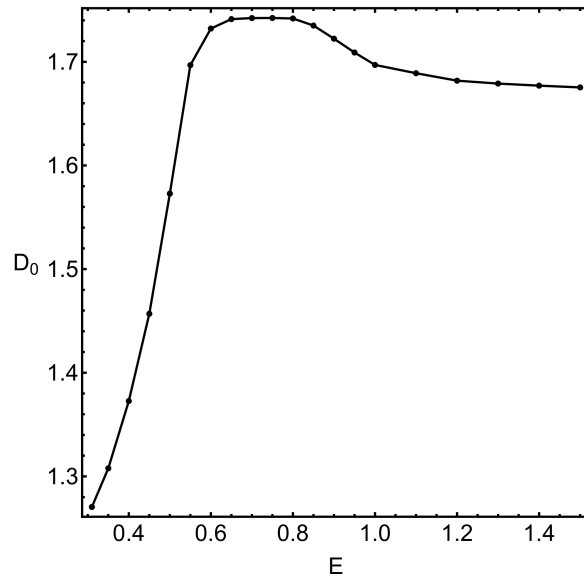


Figure 6. Evolution of the numerical value of the uncertainty dimension of the configuration plane (x, y) , as a function of E .

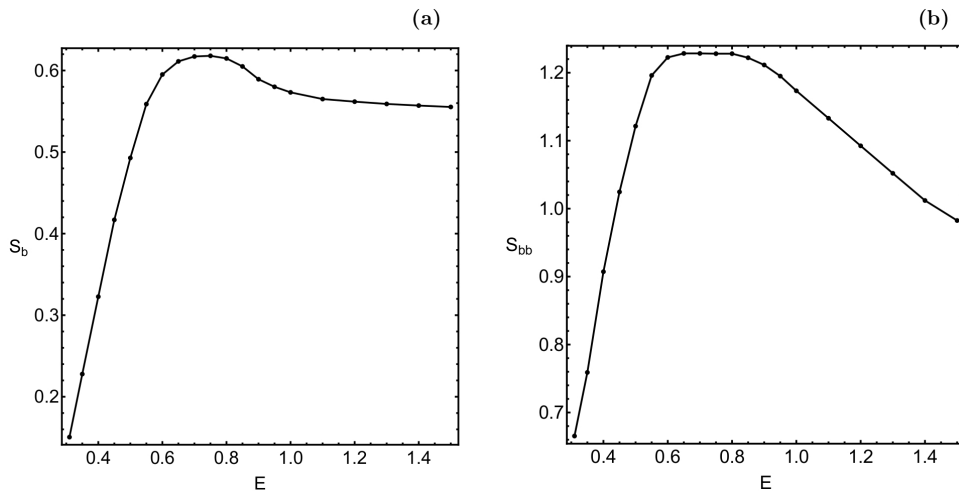


Figure 7. Evolution of the numerical value of the (a-left): basin entropy (S_b) and (b-right): boundary basin entropy (S_{bb}), of the configuration plane (x, y) , as a function of E .

2D plane, it is assumed to be the reason of this impressive coincidence of their parametric evolution.

According to the “log 2 criterion”, the boundaries of the basins are fractal if the boundary basins entropy $S_{bb} > \log 2$. In part (b) of Fig. 7 we demonstrate how the boundary basin entropy S_{bb} evolve, as a function of E . One can see, that the basin boundaries on the configuration plane (x, y) are always fractal, because $S_{bb} > \log 2$ when $E \in (0, 1.5]$. In the energy interval $(0, 0.8)$ the parametric evolution of both S_b and S_{bb} is very similar, while for higher values of E ($E > 0.8$) the boundary basin

entropy displays an almost linear drop, in contrast to the almost constant evolution of the respective basin entropy.

5. Discussion

The escape dynamics of a Hamiltonian system with five channels of escape have been numerically investigated by classifying starting conditions of orbits. We successfully determined the influence of the total energy on the character of the orbits. Additionally, we connected the basins of escape with the corresponding distributions of the time of the escape of the orbits. The degree of the fractality of the dynamical systems has been measured by calculating both the uncertainty (fractal) dimension as well as the (boundary) basin entropy. As far as we know, this is the first work containing quantitative information about the degree of the fractality of a dynamical system with five channels of escape.

In [15, 16] we had also numerically investigated the escape dynamics in multi-channel Hamiltonian systems. However in the present paper we used a more realistic choice of initial conditions. To be more precise, in our previous studies, the choice of the initial conditions was not able to display the fact that all the escape channels of the system are in fact equiprobable. Using the particular choice of starting conditions in the present paper, we managed to correctly, illustrate that the amount of escaping orbits is exactly the same for all five escape channels.

The Hamiltonian with the five channels of escape may represent realistic physical systems where rearrangement multichannel scattering occurs. In one case, potential holes with several exit channels appear in reactive scattering, for example in nuclear scattering and in molecular scattering. The same effective potential may also be used in astronomical systems, where classical Hamiltonian dynamics is the appropriate form of description. For instance, we may consider the case of a star coming close to a double or even better a triple star system and causing the rearrangement of the stars.

For numerically integrating the grids of starting conditions we used a Bulirsch-Stoer routine in standard FORTRAN 77 (e.g., [52]), with double precision. The required CPU time, per grid, was varying between 12 and 27 hours, using a Quad-Core i7 vPro 4.0 GHz processor. All the graphics of the article have been constructed by using the 11.3 version of the Mathematica[®] software [53].

References

- [1] R. Barrio, F. Blesa and S. Serrano, *Bifurcations and safe regions in open Hamiltonians*, New Journal of Physics, 2009, 11, 053004-1-053004-12.
- [2] S. R. Bishop and M. J. Clifford, *The use of manifold tangencies to predict orbits, bifurcations and estimate escape in driven systems*, Chaos Solitons Fractals, 1996, 7, 1537-1553.
- [3] G. Contopoulos, *Asymptotic curves and escapes in Hamiltonian systems*, Astronomy and Astrophysics, 1990, 231, 41-55.
- [4] G. Contopoulos, *Order and Chaos in Dynamical Astronomy*, Springer, Berlin, 2002.
- [5] G. Contopoulos and D. Kaufmann, *Types of escapes in a simple Hamiltonian system*, Astronomy and Astrophysics, 1992, 253, 379-388.

- [6] G. Contopoulos, H. E. Kandrup and D. Kaufmann, *Fractal properties of escape from a two-dimensional potential*, Physica D, 1993, 64, 310-323.
- [7] A. Ernst and T. Peters, *Fractal basins of escape and the formation of spiral arms in a galactic potential with a bar*, Monthly Notices Of The Royal Astronomical Society, 2014, 443, 2579-2589.
- [8] C. Jung and T. Tél, *Dimension and escape rate of chaotic scattering from classical and semiclassical cross section data*, Journal of Physics A, 1991, 24, 2793-2805.
- [9] H. E. Kandrup, C. Siopis, G. Contopoulos and R. Dvorak, *Diffusion and scaling in escapes from two-degrees-of-freedom Hamiltonian systems*, Chaos, 1999, 9, 381-392.
- [10] J. F. Navarro and J. Henrard, *Spiral windows for escaping stars*, Astronomy and Astrophysics, 2001, 369, 1112-1121.
- [11] J. Schneider and T. Tél and Z. Neufeld, *Dynamics of "leaking" Hamiltonian systems*, Physical Review E, 2002, 66, 066218.
- [12] H. B. Stewart, J. M. T. Thompson, Y. Ueda and A. N. Lansbury, *Optimal escape from potential wells-patterns of regular and chaotic bifurcation*, Physica D: Nonlinear Phenomena, 1995, 85, 259-295.
- [13] J. M. T. Thompson, *Chaotic behavior triggering the escape from a potential well*, Proceedings of the Royal Society of London. Series A, 1989, 421, 195-225.
- [14] E. E. Zotos, *A Hamiltonian system of three degrees of freedom with eight channels of escape: the great escape*, Nonlinear Dynamics, 2014, 76, 1301-1326.
- [15] E. E. Zotos, *Escapes in Hamiltonian systems with multiple exit channels: part I*, Nonlinear Dynamics, 2014, 78, 1389-1420.
- [16] E. E. Zotos, *Escapes in Hamiltonian systems with multiple exit channels: part II*, Nonlinear Dynamics, 2015, 82, 357-398.
- [17] E. E. Zotos, *Fractal basin boundaries and escape dynamics in a multiwell potential*, Nonlinear Dynamics, 2016, 85, 1613-1633.
- [18] J. M. Seoane and M. A. F. Sanjuán, *New Developments in Classical Chaotic Scattering*, Reports on Progress in Physics, 2013, 76, 016001.
- [19] Q. Chen, M. Ding and E. Ott, *Chaotic scattering in several dimensions*, Physics Letter A, 1990, 145, 93-100.
- [20] M. Ding, C. Grebogi, E. Ott and J. A. Yorke, *Transition to chaotic scattering*, Physical Review A, 1990, 42, 7025-7040.
- [21] C. Jung, *Iterated scattering map for rearrangement scattering*, Journal of Physics A, 1991, 24, 1741-1750.
- [22] C. Jung, C. Mejia-Monasterio and T. H. Seligman, *Scattering one step from chaos*, Physics Letter A, 1995, 198, 306-314.
- [23] C. Jung and S. Pott, *Classical cross section for chaotic potential scattering*, Physics Letter A, 1989, 22, 2925-2938.
- [24] C. Jung and P. H. Richter, *Classical chaotic scattering-periodic orbits, symmetries, multifractal invariant sets*, Physics Letter A, 1990, 23, 2847-2866.
- [25] S. Bleher, C. Grebogi, E. Ott and R. Brown, *Fractal boundaries for exit in Hamiltonian dynamics*, Physical Review A, 1988, 38, 930-938.

- [26] J. Kennedy and J. A. Yorke, *Basins of Wada*, Physica D, 1991, 51, 213-225.
- [27] L. Poon, J. Campos, E. Ott and C. Grebogi, *Wada basins boundaries in chaotic scattering*, International Journal of Bifurcation Chaos, 1996, 6, 251-266.
- [28] F. Blesa, J. M. Seoane, R. Barrio and M. A. F. Sanjuán, *To escape or not to escape, that is the question - Perturbing the Hénon-Heiles Hamiltonian*, International Journal of Bifurcation Chaos, 2012, 22, 1230010.
- [29] J. M. Seoane, J. Aguirre and M. A. F. Sanjuán, *Basin topology in dissipative chaotic scattering*, Chaos, 2006, 16, 023101.
- [30] J. M. Seoane, M. A. F. Sanjuán and Y. C. Lai, *Fractal dimension in dissipative chaotic scattering*, Physical Review E, 2007, 76, 016208.
- [31] J. M. Seoane, L. Huang, M. A. F. Sanjuán and Y. C. Lai, *Effects of noise on chaotic scattering*, Physical Review E, 2009, 79, 047202.
- [32] J. M. Seoane and M. A. F. Sanjuán, *Escaping dynamics in the presence of dissipation and noisy in scattering systems*, International Journal of Bifurcation Chaos, 2010, 9, 2783-2793.
- [33] E. E. Zotos, *Fractal basins of attraction in the planar circular restricted three-body problem with oblateness and radiation pressure*, Astrophysics and Space Science, 2016, 361, 181.
- [34] E. E. Zotos, *Revealing the basins of convergence in the planar equilateral restricted four-body problem*, Astrophysics and Space Science, 2017, 362, 2.
- [35] E. E. Zotos and M. S. Suraj, *Basins of attraction of equilibrium points in the planar circular restricted five-body problem*, Astrophysics and Space Science, 2018, 363, 20.
- [36] J. Aguirre, J. C. Vallejo and M. A. F. Sanjuán, *Wada basins and chaotic invariant sets in the Hénon-Heiles system*, Physical Review E, 2001, 64, 066208.
- [37] R. Barrio, F. Blesa and S. Serrano, *Fractal structures in the Hénon-Heiles Hamiltonian*, Europhysics Letters, 2008, 82, 10003.
- [38] J. Nagler, *Crash test for the Copenhagen problem*, Physical Review E, 2004, 69, 066218.
- [39] J. Nagler, *Crash test for the restricted three-body problem*, Physical Review E, 2005, 71, 026227.
- [40] J. Nagler, Krieger, M. Linke, M. Schönke, J. and Wiersig, J., *Leaking billiards*, Physical Review E, 2007, 75, 046204.
- [41] E. G. Altmann, J. S. E. Portela and T. Tél, *Leaking Chaotic Systems*, Reviews of Modern Physics, 2013, 85, 869-918.
- [42] J. R. Taylor, *Scattering theory*, Wiley, New York, 1972.
- [43] R. G. Newton, *Scattering theory of waves and particles*, 2nd Edition, Springer, New York, 1982.
- [44] R. Blümel and U. Smilansky, *Random-matrix description of chaotic scattering: Semi-classical approach*, Physical Review Letters, 1990, 64, 241-244.
- [45] B. Eckhardt, *Irregular scattering*, Physica D, 1988, 33, 89-98.
- [46] C. Jung, *Iterated scattering map for rearrangement scattering*, Journal of Physics A, 1991, 24, 1741-1750.

-
- [47] C. Skokos, *Alignment indices: A new, simple method for determining the ordered or chaotic nature of orbits*, Journal of Physics A: Mathematical and General, 2001, 34, 10029-10043.
- [48] J. Aguirre, R. L. Viana and M. A. F. Sanjuán, *Fractal Structures in nonlinear dynamics*, Reviews of Modern Physics, 2009, 81, 333-386.
- [49] E. Ott, *Chaos in Dynamical Systems*, Cambridge University Press, Cambridge, 1993.
- [50] A. Daza, A. Wagemakers, B. Georgeot, D. Guéry-Odelin, and M. A. F. Sanjuán, *Basin entropy: a new tool to analyze uncertainty in dynamical systems*, Scientific Reports, 2016, 6, 31416.
- [51] E. E. Zotos, *On the Newton-Raphson basins of convergence of the out-of-plane equilibrium points in the Copenhagen problem with oblate primaries*, International Journal of Non-Linear Mechanics, 2018, 103, 93-103.
- [52] H. P. Press, S. A. Teukolsky, W. T. Vetterling and B. P. Flannery, *Numerical Recipes in FORTRAN 77*, 2nd Edition, Cambridge University Press, Cambridge, 1992.
- [53] S. Wolfram, *The Mathematica Book*, Wolfram Media, Champaign, 2003.